Journal of Marine Science and Technology (2021) 26:190–200
https://doi.org/10.1007/s00773-020-00728-3

ORIGINAL ARTICLE

Influence of heave plates on the dynamics of a floating offshore wind turbine in waves

Pedro C. Mello[1] · Edgard B. Malta[2] · Raíza O. P. da Silva[1] · Matheus H. O. Candido[1] · Lucas Henrique S. do Carmo[1] · Izabela F. Alberto[1] · Guilherme R. Franzini[3] · Alexandre N. Simos[1] · Hideyuki Suzuki[4] · Rodolfo T. Gonçalves[4]

Received: 29 September 2019 / Accepted: 23 April 2020 / Published online: 14 May 2020

Abstract
This paper presents an analysis of the effects of heave plates with large skirts on the dynamics of a semi-submersible FOWT in waves. The analysis was based on a preliminary hull configuration envisaged for Brazilian waters. A numerical model based on linear frequency-domain hydrodynamics evaluated with panel methods was used for predicting the effects of the heave plates on the natural periods of motions. The predictions were compared to the results of model tests conducted in a wave basin involving ten different configurations of plate diameters and skirt heights. The experimental results confirmed the validity of the numerical predictions and provided quantitative results regarding the variations in viscous damping associated with the dimensions of the heave plates. The data will be used for future calibration of a parametric model for hull geometry optimization.

Keywords FOWT dynamics · Heave plates · Seakeeping model tests

1 Introduction

Floating Offshore Wind Turbines (FOWTs) are quickly moving from a stage of "demonstration technology" to wide acceptance in commercial grid-connected large-scale wind farms. This movement reflects the fact that, by now, this technology is unquestionably seen as the main alternative for rapidly expanding the potential of offshore wind power generation. At first, the concepts for the floaters that support the turbine were mainly derived from the offshore oil and gas field, as spars, semi-submersibles, tension-leg platforms (TLPs), or their variations of them. More recently, however, some new proposals for hull geometry have also been tested as promising alternatives for reducing the motions of the turbines induced by waves. An excellent account of the current scenario regarding the floater's design can be found, for instance, in Ref. [1].

In this continuously evolving scenario of diverse hull geometries, the semi-submersible concept based on vertical cylindrical columns, with or without pontoons for additional floatation, remains one of the most recurrent, a fact illustrated by many concepts, such as the well-known Windfloat, see Refs. [2, 3]. In the context of semi-submersible floaters, two features always pursued in the FOWT design for reducing its motions in waves are: first, increasing the natural periods of motions in the vertical plane (associated to the heave, roll and pitch motions of the floater); and second, enlarging the hydrodynamic viscous damping related to these motions. Both objectives can be targeted by the use of heave-plates and, therefore, this alternative has become quite standard for FOWT designs based on semi-submersible hulls, especially for those that do not adopt horizontal pontoons. Examples of designs for which the heave plates (or the so-called water-entrapment plates) are deemed the main devices responsible for improving the hydrodynamic behavior of the hull are given in Refs. [4-6].

✉ Rodolfo T. Gonçalves
goncalves@edu.k.u-tokyo.ac.jp

1 TPN, Numerical Offshore Tank Laboratory, Department of Naval Architecture and Ocean Engineering, Escola Politécnica, University of São Paulo, São Paulo, SP, Brazil

2 Technomar, Engenharia Oceânica, São Paulo, SP, Brazil

3 LMO, Offshore Mechanics Laboratory, Department of Mechanical Engineering, Escola Politécnica, University of São Paulo, São Paulo, SP, Brazil

4 OSPL, Ocean Space Planning Laboratory, Department of Systems Innovation, School of Engineering, The University of Tokyo, 7-3-1 Hongo, Bunkyo-Ku, Tokyo 113-8656, Japan

Since the sensitivity of the FOWT motions response in waves with respect to the dimensions of the heave plates is usually large, many studies evaluating the impact of the heave plates geometry on this response have been presented recently, as in Refs. [7-9]. In these works, an account on the variation in added mass and damping with geometrical parameters of the plates (including thickness, reinforcements and the use of skirts on the edges) under different ranges of Keulegan-Carpenter numbers (KC) can be found. Other important issues are also discussed in the literature, such as the possible scale effects involved in the experimental tests of heave plates [10] and the influence of the proximity to the seabed on the performance of the heave plates [11].

In the present paper, an analysis concerning the adoption of heave plates with large skirts is presented. The work was developed in the context of the conception of a FOWT designed to operate in Brazilian waters, a collaborative research being conducted by the University of São Paulo (USP), Brazil, and the University of Tokyo, Japan, see details in Ref. [12]. The preliminary version of the hull consists of four vertical columns of different diameters, and it was designed to ensure proper hydrostatic stability and positive floatability in case of hull damage. Heave plates were positioned at the bottom of each column, and vertical skirts on the edges of each plate were used to provide a finer tuning of the natural periods of motions (heave, roll, and pitch), without the need for further increasing the diameter of the plates. The final design of the hull will be based on an optimization procedure involving motion accelerations of the rotor-nacelle assembly (RNA) and costs, which, in turn, will rely on a linear (frequency-domain) hydrodynamic model.

Therefore, one of the main objectives of the current analysis is to verify whether or not the wave-frequency motions of the floater (1st order motions) can be adequately predicted by means of a linear radiation-diffraction analysis, taking apart the effects of viscous-damping on the resonant amplifications. Another important goal is to provide experimental data for establishing a procedure for anticipating the viscous damping levels based on the sea conditions to be analyzed, something that is also being pursued in other FOWT geometries [13]. To achieve these goals, robust experimental data are necessary, meaning data that show the trends of variations in motion response with respect to the heave plates dimensions clearly. For this reason, small-scale models of the heave plates were made considering an extensive range of diameters and skirt heights, including some that are known to be much larger than the ones that will eventually be selected for the actual design.

As a first step in this investigation, the results comprising viscous damping levels (both linear and quadratic) and natural periods of motions are presented based on decay tests, and the linear response amplitude operator (RAOs) of the 6d of motions of the floater obtained both from regular waves and white-noise irregular waves. The experimental results for natural periods and RAOs were compared to those predicted by software WAMIT®, in which the heave plates with skirts were modeled using dipole panels. The level of agreement obtained between the numerical predictions and model tests results showed to be acceptable in general. Particularly, the results for the viscous damping showed interesting features regarding the effects of skirt height and will be used in the continuation of this research for tuning the prediction of damping in the context of the parametric hull optimization.

2 Methodology

A numerical model based on the radiation-diffraction code WAMIT® was adopted to evaluate the impact of the heave plates on the added mass and natural periods of motions, after comparisons with the tests of the floater in regular and irregular waves indicated that the potential flow model was indeed capable of providing proper estimates of such parameters. The following sections first present a brief description of the FOWT geometry (Sect. 2.1), followed by a discussion of the procedures adopted for the numerical modeling (Sect. 2.2) and the main aspects of the experimental setup (Sect. 2.3).

2.1 FOWT geometry

The preliminary version of the FOWT presented a configuration with four columns in a triangular shape, with the center column being wider than the side columns, Fig. 1. The main

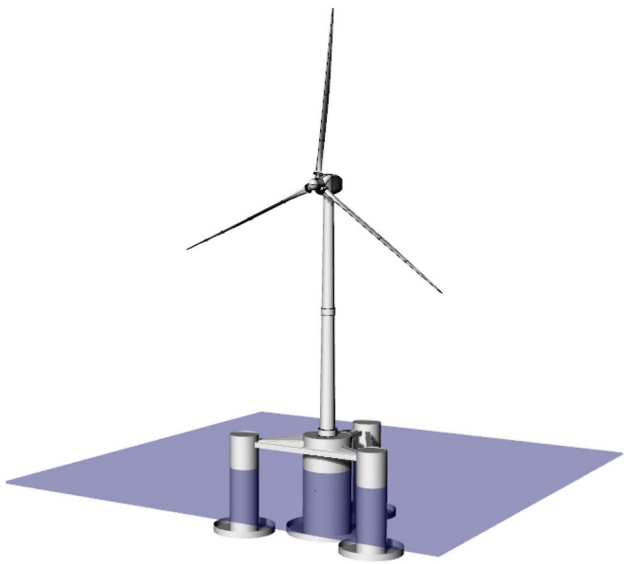

Fig. 1 FOWT with heave plates

purpose of this configuration was to guarantee stability margins in flooded conditions and also to provide proper hydrostatic lever arm for compensating the rotor thrust. At the present stage of the research, the adopted benchmark model of the turbine was the National Renewable Energy Laboratory (NREL) 5 MW turbine, considering rotor diameter and a tower height of the NREL OC4 design, see details in Ref. [14].

Heave plates were adopted to help detuning heave, roll and pitch natural frequencies from the wave frequency range with the highest energy, and also to increase the viscous damping of the vertical motions. Model tests with parametric variations in the plate diameters and skirt heights were conducted in a wave basin aiming at studying the influence of the heave plates on the FOWT dynamics in waves. For this, three different widths of the plates were combined to three different skirt heights, thus comprising a total of nine different heave plate configurations (including a version of the model without heave plates also tested for comparison purposes). Table 1 presents the main dimensions of FOWT, both in full and model scales (1:80). The heave plates geometry is illustrated in Fig. 2. The width and skirt height dimensions of the plates were the same for all four columns. The constructive design of the model maintained a similarity with the full-scale design, the experimented model in the reduced scale can be seen in Fig. 3. Ballast weights were positioned inside the columns to calibrate the center of gravity and inertia of the model. Aluminum bars connected the columns on the upper side of the model and to the tower. At the top of the tower, a mass represented the equivalent nacelle and rotor mass, although no attempt was made at this stage to represent the inertia of the rotor-nacelle assembly.

2.2 Numerical model

The numerical evaluation of the FOWT linear motion dynamics was carried out using WAMIT®, a code that uses panel methods to solve the radiation-diffraction problem. The hull surfaces were generated using the CAD software Rhinoceros®. The submerged geometry of the columns was represented by high-order surfaces, while the heave plates were modeled as zero-thickness discs utilizing dipole panels since the actual thickness of these elements was quite small. For generating the numerical mesh, a characteristic length of 4 m was adopted, resulting in a system with approximately 1400 equations. A prior convergence analysis was made,

Table 1 Main properties of the FOWT

	Full scale	Model scale
Diameter of center column	15 m	187.5 mm
Diameter of side column	9 m	112.5 mm
Draft	20 m	250 mm
Nacelle weight	150 t	0.293 kg
Tower weight	200 t	0.391 kg
Displacement	7351 t	14.300 kg
KG (from the bottom)	14.00 m	175 mm
Gyradius Rxx and Ryy	25.80 m	322 mm
Gyradius Rzz	20.70 m	259 mm
Heave plates width	4–6 m	50–75 mm
Heave plates skirt height	4–6 m	50–75 mm

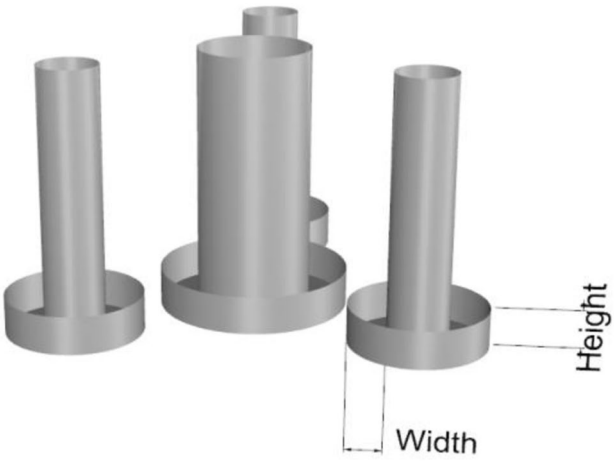

Fig. 2 Heave plate geometry parameters

Fig. 3 Picture of the reduced scale model

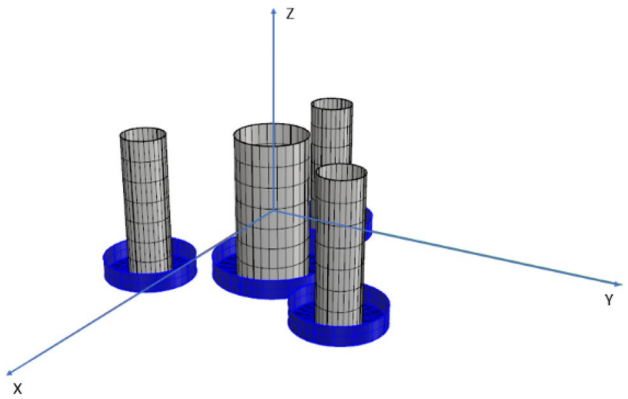

Fig. 4 High-order mesh of columns and heave plates

which ensured that this mesh provided a proper representation for the first-order hydrodynamic analysis (Fig. 4).

The FOWT mass/inertia matrix was previously evaluated based on a stability model. This model contains all the data concerning loading, ballast and the lightweight of the hull, tower, and RNA. The mass matrix (M) was then used as input in WAMIT for obtaining the motion Response Amplitude Operators (RAO) for each wave frequency (ω) and direction of incidence (θ) (Eq. 1).

Among the several properties that can be evaluated with the WAMIT® code, in the scope of this study mainly the following properties were analyzed: added mass (A), external damping (B) and external stiffness (C).

$$\mathrm{RAO}(\omega,\theta)=\frac{X(\omega,\theta)}{-\omega^2(M+A(\omega))+i\omega(B^{\mathrm{pot}}(\omega)+B)+C^{\mathrm{hydro}}+C} \quad (1)$$

Together with the added mass matrix (A), the potential damping (B^{pot}), the hydrostatic restoring (C^{hydro}) and the wave exciting forces (X) were all computed by the numerical method and used by WAMIT® code to generate the RAO curves.

The mass/inertia matrix adopted in the computations is presented in Table 2. The same mass/inertia configuration was representative for all the heave plates combinations, something that was guaranteed by adjusting the ballasts of each configuration in the model tests.

The external stiffness matrix was computed to represent the horizontal mooring system adopted in the model tests, as in Table 3. More details about the mooring arrangement will be provided in the following sections.

In addition to the potential damping, the analysis of this kind of floater requires the inclusion of an external (linearized) damping matrix in the RAO computations. This procedure is necessary for adjusting the resonant motions in the degrees of freedom since the viscous effects were not evaluated by a potential theory, such as those that involve vertical motions of the heave plates.

A well-known drawback of the linear hydrodynamic analysis is that, due to the inherently nonlinear nature of the viscous drag, the external damping matrix will depend on the amplitudes of body motion. For comparison purposes only, the RAOs presented in Figs. 5 and 6 were all evaluated considering a damping ratio of 4% of the critical damping for the heave motion RAOs and 2% of the critical damping for all the other motions. The corresponding dimensional damping coefficients are provided in Table 4.

The results as follows will be restricted to surge, heave, and pitch motions, for comparison with the tests in bow waves that will be discussed in Sect. 4. Note that, due to the hull configuration, the values for roll and pitch were quite similar. Also, in Table 4, as well as for all the other results presented next, the width of the heave plates is denoted by L and the height of the skirt by H, followed by the value of the

Table 2 Mass (Kg) and Inertia (Kgm^2) matrix

7.35E+06	0	0	0	0	0
0	7.35E+06	0	0	0	0
0	0	7.35E+06	0	0	0
0	0	0	4.88E+09	− 2.00E+06	1.57E+07
0	0	0	− 2.00E+06	4.88E+09	2.42E+06
0	0	0	1.57E+07	2.42E+06	3.15E+09

Table 3 External stiffness matrix, units in (Nm^{-1}) and (Nm^2)

8.80E + 04	0	0	0	0	0
0	8.80E+04	0	0	0	0
0	0	3.49E+03	0	0	0
0	0	0	1.05E+08	0	0
0	0	0	0	1.05E+08	0
0	0	0	0	0	4.39E+08

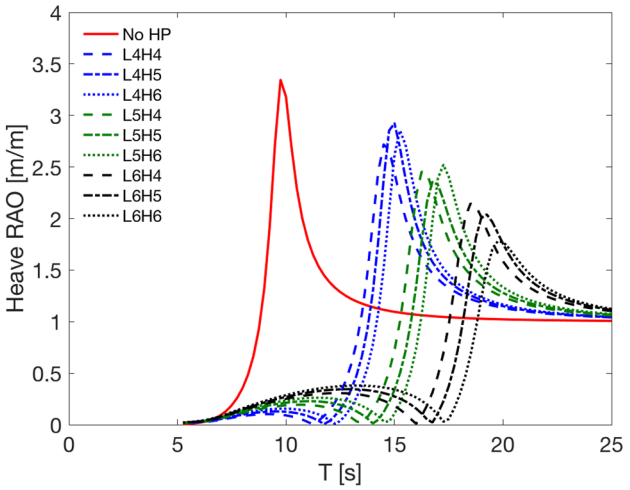

Fig. 5 Numerical heave RAO for each heave plate

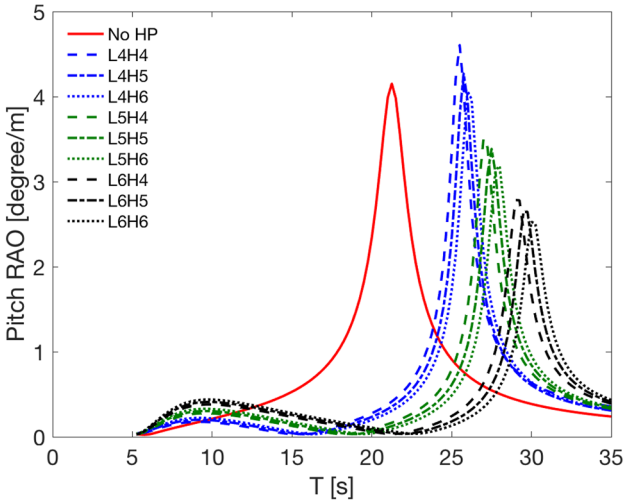

Fig. 6 Numerical pitch RAO for each heave plate

Table 4 External damping coefficients for different heave plates obtained from numerical calculations

	$B_{11} \times 10^5$ (kg/s)	$B_{33} \times 10^5$ (kg/s)	$B_{55} \times 10^8$ (kg m^2/s)
L0H0	1.08	3.48	1.23
L4H4	1.13	7.49	0.74
L5H4	1.15	8.37	0.79
L6H4	1.16	9.45	0.85
L4H5	1.15	6.83	0.75
L5H5	1.17	8.60	0.80
L6H5	1.19	9.73	0.86
L4H6	1.18	6.98	0.76
L5H6	1.21	7.84	0.81
L6H6	1.23	11.11	0.88

Table 5 Added mass coefficients for different heave plates obtained from numerical calculations

	$A_{11} \times 10^6$ (kg)	$A_{33} \times 10^6$ (kg)	$A_{55} \times 10^9$ (kg)
L0H0	6.00	1.97	0.35
L4H4	7.28	11.90	2.66
L5H4	7.66	16.60	3.68
L6H4	8.02	23.20	5.03
L4H5	7.83	12.80	2.88
L5H5	8.37	17.90	3.97
L6H5	8.89	25.10	5.39
L4H6	8.48	13.70	3.09
L5H6	9.22	19.20	4.25
L6H6	9.93	26.90	5.76

Table 6 Surge, heave, and pitch natural periods obtained from numerical calculations

	Tn1 (s)	Tn3 (s)	Tn5 (s)
Model 0–L0H0	77.52	10.10	21.31
Model 1–L4H4	81.16	14.50	25.63
Model 2–L5H4	82.21	16.18	27.27
Model 3–L6H4	83.19	18.28	29.34
Model 4–L4H5	82.65	14.86	25.97
Model 5–L5H5	84.12	16.63	27.72
Model 6–L6H5	85.50	18.83	29.88
Model 7–L4H6	84.43	15.19	26.32
Model 8–L5H6	86.38	17.06	28.16
Model 9–L6H6	88.21	19.35	30.40

respective dimension in meters (thus, as an example, L4H5 denotes the model with heave plate width of 4 m and skirt height of 5 m in full scale).

Table 5 presents the values of the added mass for each heave plate configuration. In these results, it is worth observing that the increase of the plate width was more effective in augmenting the added mass if compared to the skirt height, something that could be anticipated. However, the variations in skirt height still resulted in changes in the added masses which were not irrelevant and, therefore, they can be envisaged as a possible alternative for a finer tuning of the natural periods, as can be seen in Table 6.

The natural periods listed in Table 6 were all estimated from the numerical model. The values for heave and pitch must be properly tuned based on the metocean conditions of the operation site in order to keep the accelerations of the rotor and nacelle within reasonable limits. The natural periods of surge reflected the stiffness of the mooring arrangement adopted in the model tests and their correct prediction was of utmost importance for the analysis of slow-drift motions, as observed by [15].

Figures 5 and 6 show a graphical representation of the RAOs obtained by numerical calculations. In these figures, it is possible to evaluate the effects that the changes in the heave plates dimensions had on the FOWT first-order dynamics. At this point, note that, for the FOWT design, not only was proper calibration of the natural periods important, but also the adjustment of the RAO minima, which happens within the wave frequency range.

2.3 Experimental setup

The experimental model tests were conducted in the Ocean Basin of the Numerical Offshore Tank Laboratory (TPN) of the University of São Paulo, Brazil, as shown in Fig. 7. The facility consists of a squared 14 m × 14 m × 4 m (length, width, depth) basin, equipped with 152 active-absorption wave generators. The equipment can generate the incident waves and absorb waves diffracted and radiated by the model, following specific control algorithms, see details in Ref. [16]. The limits for wave generation comprise a peak period range from about 0.8 s up to 2.5 s. Therefore, to achieve the intended peak periods, the model tests were designed in 1:80 scale. At this stage of the research, no considerations were made about the water depth (corresponding to 320 m in this scale, much larger than the one expected for the real design) and wind effects.

The offsets of the model were restricted using a horizontal mooring system composed of three lines with springs attached to the tank borders, as in Fig. 8. Each line connected to fairleads on the side of the model columns. The vertical position of the fairleads was close to the vertical position of the center of gravity of the model. Since the campaign also comprised tests for investigating the drifts of the platform, the equivalent stiffness in the horizontal plane was chosen to be the representative of the one expected for the final design. The adjustment was driven by the springs

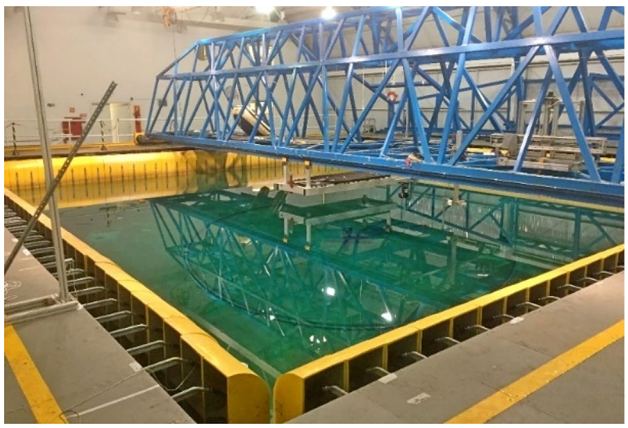

Fig. 7 Ocean basin of TPN

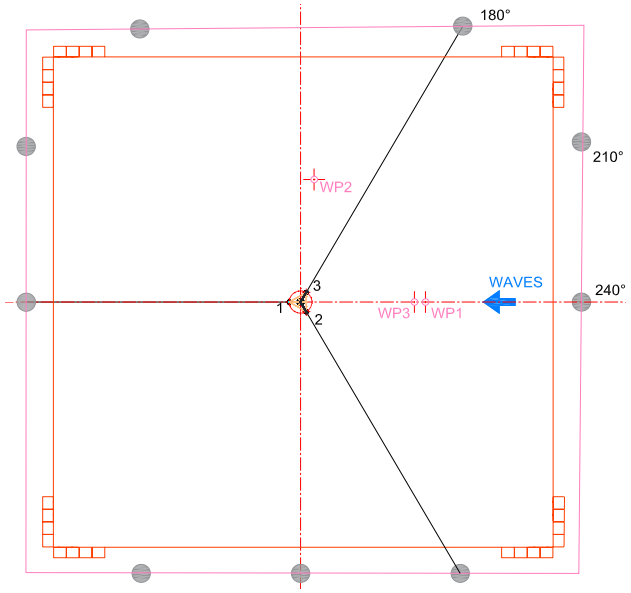

Fig. 8 Wave basin anchor and model arrangement

characteristics and the angles of the lines, which was always 120° between each line. The stiffness of each spring corresponded to 56.32 kN/m in full scale. In the real scale, the vertical elevation of connection points at tank borders corresponded to 66 m above the waterline.

Three wave probes (WP01–WP03) were employed to measure the waves during the tests, and their positions are indicated in Fig. 8. A fourth wave probe was positioned at the model location during wave calibration as wave reference and later removed for the model tests.

The model motions were measured by a Qualisys® optical tracking system positioned above the model in the instrumentation bridge. Four tracking cameras with five passive markers on the base of the model tower were used to provide accuracy and reliability for the motion measurement. Because of the redundancy of cameras on tracking each marker, the position error measurement was less than 1.0 mm. The tracking system measures the six degrees of freedom of the model (surge, sway, heave, roll, pitch, and yaw) with the center of coordinates corresponding to the platform center of gravity. The sampling frequency adopted during the measurements was 100 Hz.

Wave tests were designed to verify the numerical RAO predictions including irregular white-noise waves and regular waves with selected periods and amplitudes. The white noise wave was employed to evaluate a wide range of frequency response of the model. The white noise wave is a low-steepness irregular wave with constant energy in the frequency span and random phases. The wave adopted in the tests comprised a period range between 6.5 s and 25 s (full scale), thus covering important RAO resonances and

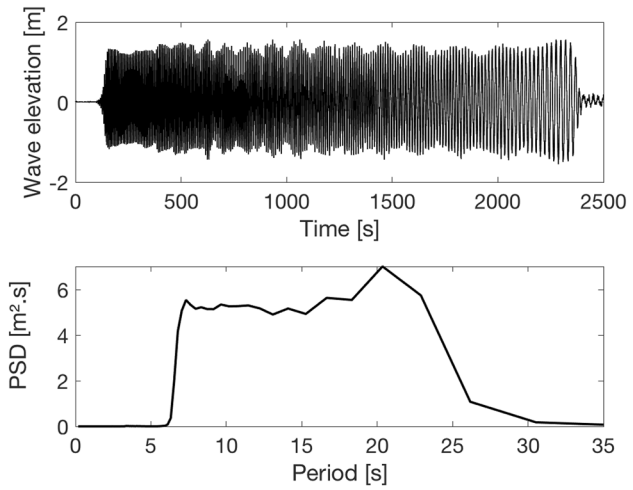

Fig. 9 White noise wave: wave elevation (above) and PSD (below)

points of minima (see Figs. 5 and 6). Figure 9 presents the white noise wave recorded and the power spectrum density (PSD) obtained from it.

In addition to the white-noise wave tests, a set of 12 regular waves with periods coincident with the heave resonance and some selected minima of the RAOs were tested with at least three different wave heights to verify nonlinear hydrodynamic effects on the model response.

3 Results

3.1 Natural periods and heave plates damping

The first quantification of natural periods and damping was obtained by means of decay tests executed in still water in the neutral position of the mooring arrangement. These tests allowed verifying the numerical predictions of natural frequencies. It was also possible to analyze the linear and the quadratic coefficients of hydrodynamic damping of the floater for the different combinations of heave plates. At least three repetitions of each decay test were carried out to reduce the statistical uncertainty associated with the experiments.

Tables 7, 8 and 9 show the average values of natural periods obtained from the tests for heave, pitch, and surge, respectively.

From the records of motion in the decay tests, it was also possible to evaluate the linear and quadratic damping coefficients for each model configuration. By comparing the results obtained for the different heave plates, the linear damping was presented as a percentage of the critical damping for each motion. Tables 10, 11 and 12 show the linear damping ratios for heave, pitch, and surge, respectively. For analysing the quadratic damping, however, the damping coefficients were presented as a percentage of the mass/inertia of each motion and, therefore, the ratios for pitch were nondimensional, but those for surge and heave

Table 7 Heave natural periods from decay tests (s)

Model ID		Width (m)			
		L0	L4	L5	L6
Skirt height (m)	H0	9.8			
	H4		14.4	16.6	18.6
	H5		15.2	16.8	19.2
	H6		15.5	17.1	19.7

Table 8 Pitch natural periods from decay tests (%)

Model ID		Width (m)			
		L0	L4	L5	L6
Skirt height (m)	H0	21.0			
	H4		25.4	27.2	29.2
	H5		25.9	27.6	29.9
	H6		26.0	27.8	30.3

Table 9 Surge natural periods from decay tests (%)

Model ID		Width (m)			
		L0	L4	L5	L6
Skirt height (m)	H0	77.9			
	H4		82.7	84.4	85.6
	H5		84.6	86.2	88.3
	H6		86.8	89.5	90.8

Table 10 Heave linear damping from decay tests (%)

Model ID		Width (m)			
		L0	L4	L5	L6
Skirt height (m)	H0	2.5%			
	H4		1.1%	0.3%	0.0%
	H5		0.2%	0.1%	0.0%
	H6		0.3%	0.7%	0.0%

Table 11 Pitch linear damping from decay tests (%)

Model ID		Width (m)			
		L0	L4	L5	L6
Skirt height (m)	H0	1.7%			
	H4		2.6%	1.1%	0.9%
	H5		1.6%	1.7%	1.4%
	H6		1.5%	1.4%	1.3%

Table 12 Surge linear damping from decay tests (%)

Model ID		Width (m)			
		L0	L4	L5	L6
Skirt height (m)	H0	1.1%			
	H4		1.4%	1.1%	2.6%
	H5		1.6%	2.0%	1.8%
	H6		1.1%	1.7%	2.0%

Table 13 Heave quadratic damping from decay tests (%)

Model ID		Width (m)			
		L0	L4	L5	L6
Skirt height (m)	H0	2.6%			
	H4		13.1%	17.8%	22.8%
	H5		14.7%	18.8%	21.0%
	H6		13.8%	14.0%	18.8%

Table 14 Pitch quadratic damping from decay tests (%)

Model ID		Width (m)			
		L0	L4	L5	L6
Skirt height (m)	H0	0.4%			
	H4		1.7%	3.9%	4.8%
	H5		2.7%	3.5%	4.1%
	H6		2.5%	3.2%	3.9%

Table 15 Surge quadratic damping from decay tests (%)

Model ID		Width (m)			
		L0	L4	L5	L6
Skirt height (m)	H0	1.5%			
	H4		4.8%	6.1%	5.6%
	H5		5.3%	6.2%	8.1%
	H6		6.4%	7.6%	8.6%

were not nondimensional form (values of the damping ratios were computed in full-scale). Tables 13, 14 and 15 show the quadratic damping ratios for heave, pitch, and surge, respectively. The method employed for evaluating the damping values is detailed in Ref. [17].

Concerning the natural periods of motion, it is possible to observe a clear increasing trend the natural periods of heave and pitch with the increasing width of the heave plates. For the ranges tested, the impact of the heave plate width was more pronounced than the one obtained when changing the skirt height, except for the surge motion. In this case, as could be anticipated, the skirt height had a more significant effect.

Table 16 Comparison of pitch natural periods (s)

Model	No ext stiffness	With ext stiffness	Experimental	Difference (%)
L0H0	24.31	21.31	21.00	1.45
L4H4	29.23	25.63	25.40	0.90
L5H4	31.10	27.27	27.20	0.26
L6H4	33.46	29.34	29.20	0.48
L4H5	29.61	25.97	25.90	0.27
L5H5	31.62	27.72	27.60	0.43
L6H5	34.07	29.88	29.90	0.07
L4H6	30.02	26.32	26.00	1.22
L5H6	32.12	28.16	27.80	1.28
L6H6	34.67	30.40	30.30	0.33

For the natural periods of surge and heave, the agreement between the values obtained from the decay tests (Tables 7, 9) with the predictions of the numerical model (Table 6) was good. The comparison indicated that the linear hydrodynamic analysis performed with the panel method was indeed capable of providing fair computations of the added mass. However, a more detailed analysis must be conducted for the pitch motion because, in this case, the effects of the horizontal mooring arrangement on the natural frequencies could not be ignored. Table 16 shows the differences observed between numerical and experimental predictions, and it is possible to note that a good agreement could only be obtained when properly considering the external stiffness matrix.

Regarding the damping, the linear damping of heave motion (Table 10) decreased with the size of the heave plates, while the quadratic damping (Table 13), increased quite strongly due to the dominating effects of viscous drag. Comparing the variations in damping with the heave plate width and skirt height, one may note that the higher damping did not occur for the larger skirt. Indeed, configuration H4L6 presented the highest damping coefficient among all the tested ones. In fact, when increasing the skirt heights above a certain threshold, the values of damping started to decrease. This behavior was due to the changes that the skirt produced in the vortex shedding pattern around the plate edges, and the same sort of trend had already been observed in the literature, as in [2]. The same trend was observed for the pitch damping (Table 14), and this behavior could be anticipated since the pitch damping was also dominated by the viscous drag associated with the quasi-vertical motions induced on the columns and heave plates.

For the surge motion (Table 15), the increase in the quadratic damping with the heave plates was not as pronounced, and it was more strongly related to the skirt heights. In this case, the largest damping values were obtained for the

largest width and height (H6L6), due to the largest projected area of the skirts in the surge direction.

3.2 Motion RAOs

Figure 10 illustrates the behavior of the pitch RAO for different stiffness configurations for the example the case of the model without heave plates (L0H0). The blue line with circle markers corresponds to the RAO obtained from the analysis of the white-noise wave test. The red line corresponds to the one predicted without considering the effects of the mooring arrangement and, in this case, one may note that the natural period of motion is clearly shifted. When considering the stiffness matrix computed in the model neutral position given in Table 3 (here denoted by Pre-tension 1), the natural period shifted and matched the experimental one quite well. However, with this change, the numerical model was not yet capable of providing a good prediction of the pitch motions in the most important wave frequency range (below 15 s). In fact, in this range the numerical predictions tended to overestimate the response observed in the experiments (Pre-tension 1). Adjustments of the stiffness matrix based on both the offsets of the platform and the levels of vertical motions of the fairleads were required to generate a new stiffness matrix able to represent the behavior of anchoring more faithfully (as in Pre-tension 2). Obviously, this is an evidence of the limitations of the linear analysis.

Contrary to the pitch, for the heave motions, the effects of the external stiffness were negligible and did not impose any notable changes on the RAO, as presented in Fig. 11 for the same model without heave plates (L0H0). The main issue involved in the proper calibration of the heave RAO was the prediction of a proper linearized external damping, which

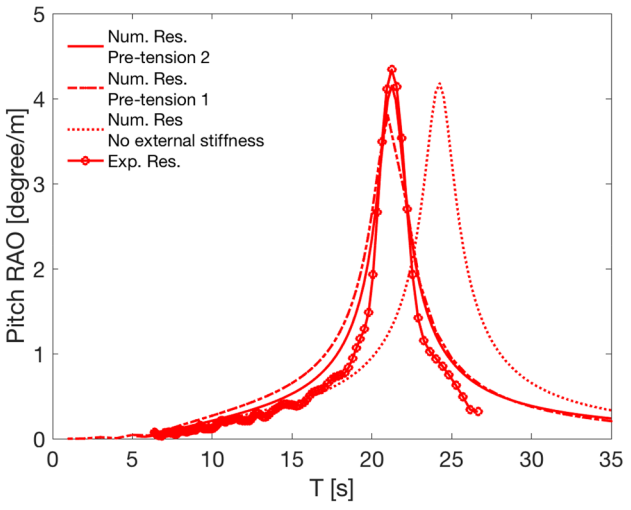

Fig. 10 Effect of the stiffness of anchoring lines on the pitch RAO. Model L0H0

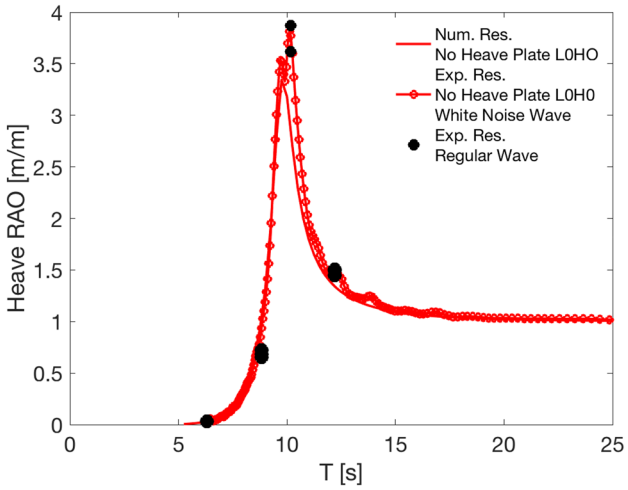

Fig. 11 Comparison of heave RAOs for model L0H0

(as mentioned before) changes with the motion amplitude. In this case, besides the results from the white-noise tests, the RAOs predicted from regular wave tests with different wave amplitudes were also presented represented by the markers in the graph. In this case, the RAO variations obtained for the different wave amplitudes were relatively low because the model without heave plates presented low damping.

Figure 12 shows the pitch RAOs obtained for the model without heave plates, the same already discussed in Fig. 10, but now also with the markers of the results from the regular wave tests. In this case, since the wave frequency range was very far from the resonant frequency, the wave amplitude had no influence on the RAOs obtained experimentally.

An illustrative example of the effects of the heave plates on the motions can be given considering the model

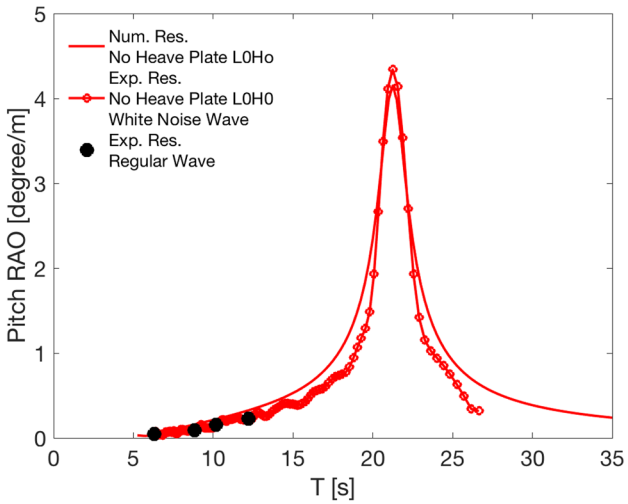

Fig. 12 Comparison of pitch RAOs for model L0H0

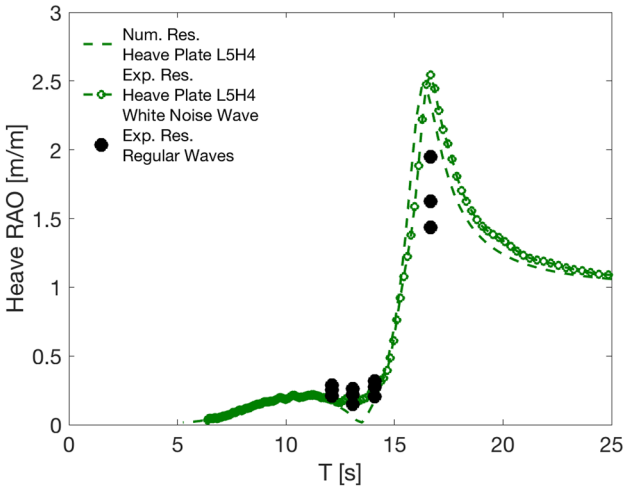

Fig. 13 Comparison of heave RAOs for model L5H4

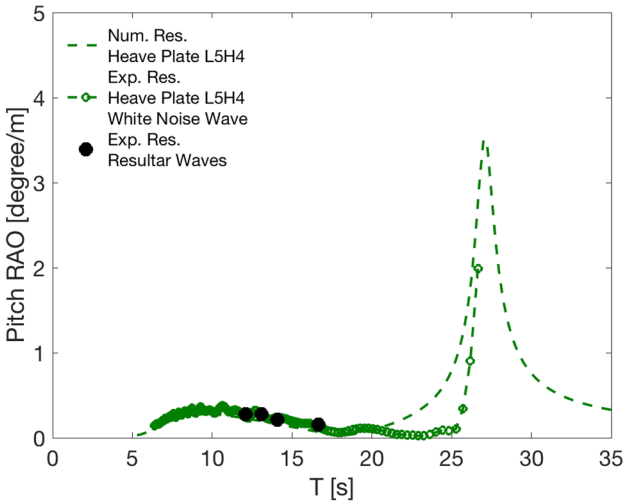

Fig. 14 Comparison of pitch RAOs for model L4H5

configuration L4H5. Figures 13 and 14 present the heave and pitch RAOs for these cases, respectively. Concerning the heave RAO, it is possible to observe that the resonant period of the heave motion was well predicted, but the cancellation point around 13 s was not observed in the experiments due to viscous drag effects. It is also possible to verify the variations of damping levels in the resonance from the results of regular waves with different amplitudes. The resonant amplification was remarkably reduced for the higher waves.

The pitch RAO of model L5H4 presented a somewhat different pattern if compared to the pitch response of model L0H0. There was a minimum amplitude of motion around the period of 18 s for L5H4 that was not observed for L0H0. In this case, the agreement between numerical and experimental values was quite reasonable up to this period, and discrepancies seemed to intensify for larger ones. However, it must be observed that, due to the shift of the natural period to a higher value imposed by the heave plates, the white-noise results above 20 s may be inaccurate.

4 Conclusions

The paper presented the first set of results concerning the effects of heave plates with large skirts on the motions of a semi-submersible FOWT. The motions were computed in the frequency domain by means of the panel code using WAMIT®, as the heave plates modeled by dipole panels. The numerical predictions were compared to a set of experimental results from model tests comprising decay tests, regular and white-noise waves.

The results confirmed that the variations in plate diameter and skirt height allowed for significant changes in the motions of the floater in waves, indicating that a parametric optimization of these dimensions may be a valuable tool for the design of the hull.

A reasonable prediction of the first-order motions could be obtained in a conventional frequency domain analysis, but the results showed that special care must be taken when considering the mooring stiffness for pitch (or roll) motions and also regarding cancellation points in the numerical RAOs since, for the latter, viscous drag effects may impose significant discrepancies on this range.

For the set of heave plates tested, the results showed that, although the plate width was the dominating dimension concerning added masses and viscous damping, variations in the skirt height can contribute to a fine tuning of the motions.

A preliminary analysis of the nonlinear viscous damping was obtained from the results of decay tests, showing that an increase in the skirt height did not always lead to a corresponding increase in the viscous damping.

The results will be used in the next steps of the research in the pursuit of a proper parametric model for predicting damping based on the characteristics of the incoming waves. For this, the experimental data will be complemented with a set of irregular wave tests. The final goal is to calibrate a parametric model based on pre-computed hydrodynamic coefficients for optimizing the hull geometry.

Acknowledgements This work was developed in the context of a Brazil-Japan collaborative research project financed by the Brazilian Coordination for the Improvement of Higher Education Personnel (CAPES) and the Japan Society for Promotion of Science (JSPS). Professors Alexandre N. Simos and Guilherme R. Franzini acknowledge their respective Research Grants from CNPq. Lucas H. S. Carmo also acknowledges CAPES for his PhD grant (Finance code-001). Mateus H. O. Candido thanks the Office of the Naval Research-Global (ONR-G) for his undergraduate scholarship (NICOP Award N62909-16-1-2066). Rodolfo T. Gonçalves thanks the JSPS for the grant as a JSPS International Research Fellow (P18355, Graduate School of Engineering, The

University of Tokyo) and also KAKENHI Grant Number JP18F18355. The Japanese team also thank the Japan Society of Naval Architects and Ocean Engineers (JASNAOE) for the opportunity and support given throughout the project "Brazil-Japan collaborative research program". The authors thank the student Matheus A. Marques (Federal University of Pernambuco, Recife, PE, Brazil) for his help during the image developments.

References

1. James R, Ros MC (2015) Floating offshore wind: market and technology review. Carbon Trust
2. Roddier D, Cermelli C, Aubault A, Weinstein A (2010) WindFloat: a floating foundation for offshore wind turbines. J Renew Sustain Energy 2:033104
3. Roddier D, Cermelli C, Aubault A, Peiffer A (2017) Summary and conclusions of the full life-cycle of the WindFloat FOWT prototype project. In: Proceedings of the ASME 2017 36th international conference on ocean, Offshore and Arctic Engineering, OMAE2017-62561, Trondheim
4. Moreno J, Cameron M, Thiagarajan KP, Mendoza (2015) CAG hydrodynamic performance of heave plates on floating offshore wind turbine platforms. In: Proceedings of the 25th international ocean and polar engineering conference, Kona
5. Yang W, Tian W, Hvalbye O, Peng Z, Wei K, Tian X (2019) Experimental Research for Stabilizing Offshore Floating Wind Turbines. Energies 12(10):1–15
6. Cermelli C, Aubault A, Roddier D, McCoy T (2010) Qualification of a semi-submersible floating foundation for multi-megawatt wind turbines. In: Proceeding of the offshore technology conference, OTC-20674-MS, Houston
7. Lopez-Pavón C, Souto-Iglesias A (2015) Hydrodynamic coefficients and pressure loads on heave plates for semi-submersible floating offshore wind turbines: a comparative analysis using large scale models. Renew Energy 81:864–881
8. Tao L, Thiagarajan K (2003) Low KC flow regimes of oscillating sharp edges I. Vortex shedding observation. Appl Ocean Res 25(1):21–35
9. Tao L, Thiagarajan K (2003) Low KC flow regimes of oscillating sharp edges. II. Hydrodynamic forces. Appl Ocean Res 25(2):53–62
10. Bezunartea A, Ruano SF, Marón-Loureiro A, Molinelli E, Moreno-Burón F, Oria-Escudero J, Riós-Tubio J, Soriano-Gomez C, Valea-Peces A, Lopez-Pavon C, Souto-Iglesias A (2020) Scale effects on heave plates for semi-submersible floating offshore wind turbines: case study with a solid plain plate. J Offshore Mech Arct Eng 142(3):031105
11. Garrido-Mendoza C, Thiagarajan K, Souto-Iglesias A, Colagrossi A, Bouscasse B (2015) Computation of flow features and hydrodynamic coefficients around heave plates oscillating near a seabed. J Fluids Struct 59:406–431
12. Gonçalves RT, Franzini GR, Simos AN, Neto AG, Mello PC, Carmo BS, Nishimoto K, Malta EB, Vieira DP CarmoLHS Amaral GA, Oliveira M, Wada R, Hirabayashi S, Suzuki H (2018) A Brazil-Japan collaboration on a conceptual design of a floating offshore wind turbine for the São Paulo Coast. In: Proceedings of the 27th international congress on waterborne transportation, shipbuilding and offshore constructions, Rio de Janeiro
13. Lemmer F, Yu W, Cheng PW (2018) Iterative frequency-domain response of floating offshore wind turbines with parametric drag. J Mar Sci Eng 6(4):118
14. Robertson A, Jonkman J, Masciola M, Goupee A, Coulling A, Luan C (2014) Definition of the semisubmersible floating system for phase II of OC4. In: Technical Report No. NREL/TP-5000-60601, National Renewable Energy Lab (NREL)
15. Simos AN, Ruggeri F, Watai RA, Souto-Iglesias A, Lopez-Pavon C (2018) Slow-drift of a floating wind turbine: an assessment of frequency-domain methods based on model tests. Renew Energy 116:133–154
16. Mello PC, Carneiro ML, Tannuri EA, Kassab F Jr, Marques RP, Adamowski JC, Nishimoto K (2013) A control and automation system for wave basins. Mechatronics 23(1):94–107
17. Malta EB, Gonçalves RT, Matsumoto FT, Pereira FR, Fujarra ALC, NishimotoK (2010) Damping coefficient analyses for floating offshore structures. In: Proceedings of the ASME 29th internatiional conference on ocean, offshore and arctic engineering, OMAE2010-20093, Shanghai